Article

Guiding Metal Organic Framework Morphology via Monolayer Artificial Defect-Induced Preferential Facet Selection

Pubali Kar, Chang-Ming Wang, Chia-Li Liao, Ta-Sheng Chang, and Wei-Ssu Liao*

Read Online

ACCESS | Metrics & More | Article Recommendations | Supporting Information

ABSTRACT: Guiding metal organic framework (MOF) morphology, especially without the need for chemical additives, still remains a challenge. For the first time, we report a unique surface guiding approach in controlling the crystal morphology formation of zeolitic imidazole framework-8 (ZIF-8) and HKUST-1 MOFs on disrupted alkanethiol self-assembled monolayer (SAM)-covered Au substrates. Selective molecule removal is applied to generate diverse SAM matrices rich in artificial molecular defects in a monolayer to direct the dynamic crystal growth process. When a 11-mercaptoundecanol alkanethiol monolayer is ruptured, the hydroxyl tail groups of surface residue molecules act as nucleating sites by coordination with precursor metal ions. Meanwhile, the exposed alkane chain backbones stabilize a particular facet of MOF nuclei in the dynamic growth by slowing down their crystal growth rates along a specific direction. The competitive formation between the [110] and [100] planes of ZIF-8 ultimately regulates the crystal shapes from rhombic dodecahedron, truncated rhombic dodecahedron, and truncated cube to cube. Similarly, changeable morphologies of HKUST-1 crystals are also achieved from cube and tetrakaidekahedron to octahedron, originating from the competitive selection between the [100] and [111] planes. In addition to the artificial matrix preferred orientation of initial nucleation, parameters such as temperature also play a crucial role in the resulting crystal morphology. Standing on the additive-free MOF crystal morphology growth control, porous architectures prepared in this approach can act as templates for ligand-free metal (Au, Ag, and Cu) nanocluster synthesis. The nanocluster-embedded MOF structures represent distinct crystal morphology-dependent optical properties, and interestingly, their fluorescence emission can be highly enhanced by facet-induced nanocluster packing alignments. These findings not only provide a unique thought on MOF crystal morphology guidance but also pave a new route for the accompanied property investigation and further application.

KEYWORDS: metal organic framework, artificial defect, self-assembled monolayer, morphology, preferential facet
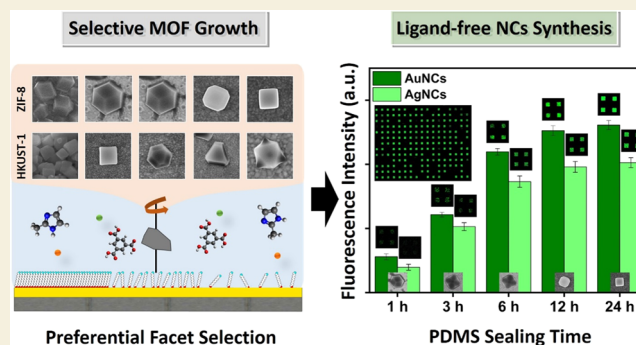
INTRODUCTION

Metal organic frameworks (MOFs) are a unique class of highly ordered solid-state porous materials, which is assembled by a three-dimensional (3D) network of metal ions coordinated to multidentate organic linkers.[1,2] Due to their large surface area, tunable pore size, and enormous thermal and chemical stability,[3] MOFs have received considerable attention in gas storage,[4] sensing,[5] drug delivery,[6] chemical separation,[7] and catalysis[8,9] applications. The exceptional properties of MOFs can be tuned by appropriate selections of metal coordination geometry and organic ligand functionality through synthetic design and material composition.[10−12] Besides, the behavior of MOFs is also morphology-dependent and can therefore be altered by post-treatments without changing the material composition.[13,14] The introduction of supplemental functionalities by these treatments may alter their morphologies based on the postsynthetic deprotonation process or the organic linker/metal ion combination.[15−17] To achieve MOF structure control and the corresponding property regulation, precise

guidance over MOF nucleation and growth processes has to be achieved. This attempt is mostly realized by precursor adjustments in the synthetic solution. For example, multi-composition approaches help to control the MOF morphology by utilizing appropriate metal sources or different metal ion/organic linker ratios in the reactant preparation.[18,19] Furthermore, a surfactant acting as the capping agent or inhibitor is able to reduce the crystal surface energy by affecting coordination equilibria and slow down the crystal growth rate for MOF morphology controls.[21,22] Although current strategies provide diverse types of MOF morphology selections, suitable precursor pairing, nucleation kinetics
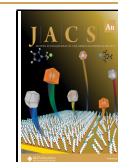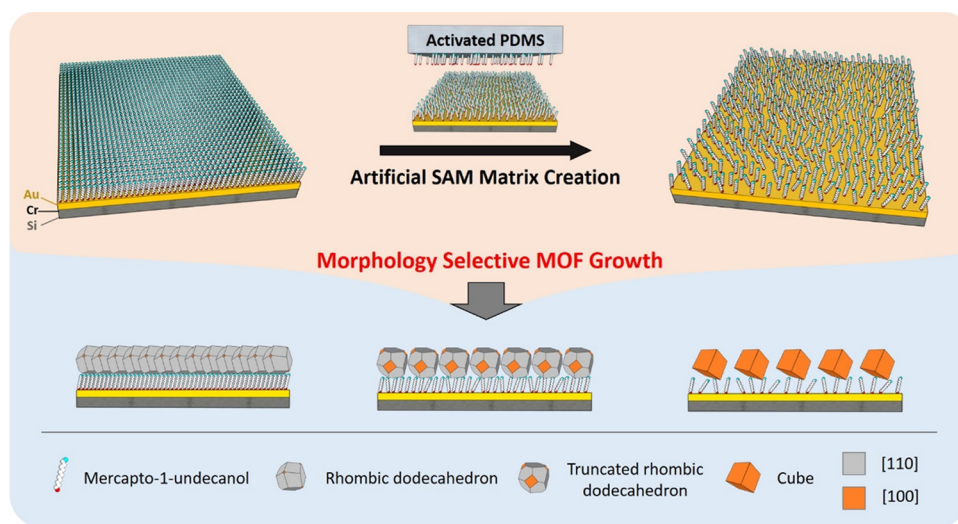
Scheme 1. Schematic Illustration of the Artificial Molecular Matrix Creation and the Resulting ZIF-8 MOF Morphology Changes via Preferential Facet Selections between the [110, Gray] and [100, Orange] Planes

control, crystallinity defect minimization, and additive reagent removal remain challenging.[23−26] A different type of MOF preparation relies on the surface-assisted growth process to achieve MOF thin-film creation. For instance, Langmuir–Blodgett operation,[27] liquid-phase epitaxy method,[28] secondary growth approach,[29] interfacial diffusion strategy,[30] and layer-by-layer synthesis[31] have been demonstrated. These strategies utilize specific chemical properties of the supporting substrate to direct heterogeneous nucleation and growth for pure MOF thin film production. However, these approaches often require tedious and time-consuming procedures,[32] and the use of specialized, toxic, and flammable organic solvents is always unavoidable.[31] Most importantly, these techniques impose poor controls over product layer thickness, molecular ordering and orientation, and crystal morphology diversity.

Material interface molecular environment can impact chemical and physical behaviors of the involved species, and its control is crucial to a substance's final representing property. To influence the interface condition, surface modification or linkage modulation is a straightforward approach and has provided practical solutions toward modern scientific or engineering issues.[33,34] Taking self-assembled monolayer (SAM) as an example, the formation of SAMs on a supporting substrate opens a new door for functionality alteration,[35] chemical/biological conjugation,[36] and material growth,[37] enabling the creation of advanced devices,[38] sensors,[39] and lithographic techniques.[40] Utilizing SAM formation to support the growth of MOFs has also been demonstrated, where uniformly oriented three-dimensional MOF thin films (ZIF-8,[28] HKUST-1,[41] and MOF-5[42,43]) are created. In these operations, the exposed alkanethiol SAM functional groups interact with metal ions and assist epitaxial crystal growth in a layer-by-layer fashion during MOF formation.[28] Due to the fixed interface interaction between SAM tail groups and the precursor solution, the crystal morphology of MOF is determined by the introduced metal ion/organic ligand recipe and cannot be further changed.

Modulation of SAM environment is not an unachievable task, but special techniques have to be employed to alter a stable interface. The simplest approach to create a heterogeneous SAM is through the use of precursor solutions containing molecules with different moieties.[44] Inserting dissimilar molecules into natural SAM defects can also lead to specific molecular alignments or a highly diluted molecular distribution.[45] Using selective molecular removal techniques, the interface molecule lift-off process enables the creation of artificial cavities in SAMs and disrupts the originally well-ordered molecular environment.[46] Specifically, the selective removal of molecules from SAMs provides a unique opportunity to generate diverse molecular matrices suitable for interface reaction controls. Chemical lift-off lithography is one such technique that achieves reliable SAM environment disruption, which removes surface molecules by utilizing the tunable covalent bond formation between an activated elastomer stamp and the alkanethiol tail groups. This enables a straightforward artificial SAM defect generation and provides a variety of sensing, molecular recognition, and physical confinement applications.[47,48] Considering the interface interaction-dependent MOF formation, a molecular environment-manipulated matrix is expected to affect the nucleating mechanism and its subsequent growth process. This should provide a unique opportunity to modulate MOF crystal morphology through interface molecular interaction guidance based on a single chemical recipe.

In this work, a surface-guiding strategy for controlling the MOF crystal morphology under a single metal/ligand recipe is introduced. An alkanethiol SAM matrix rich in artificial defects is prepared by selective Au−thiolate removal. The residual hydroxyl-terminated alkanethiol tail groups act as nucleation sites for zeolitic imidazole framework-8 (ZIF-8) MOF crystal growth, where the hydrophobic alkane chain exposed via partial SAM removal provides a preferential selection toward MOF crystal facets. This finely tunable artificial molecular matrix enables progressive alteration of ZIF-8 crystals from rhombic dodecahedron, truncated rhombic dodecahedron, and truncated cube to cube shapes. With similar substrates created under the same concept, HKUST-1 MOFs with changeable morphologies from cubic, and tetrakaidekahedral to octahedral can also be prepared using this unique preferential facet-selective guiding approach. The origin of this selective facet control is attributed to the ratio balance between nucleating sites to exposed alkane chains in the dynamic crystal growth
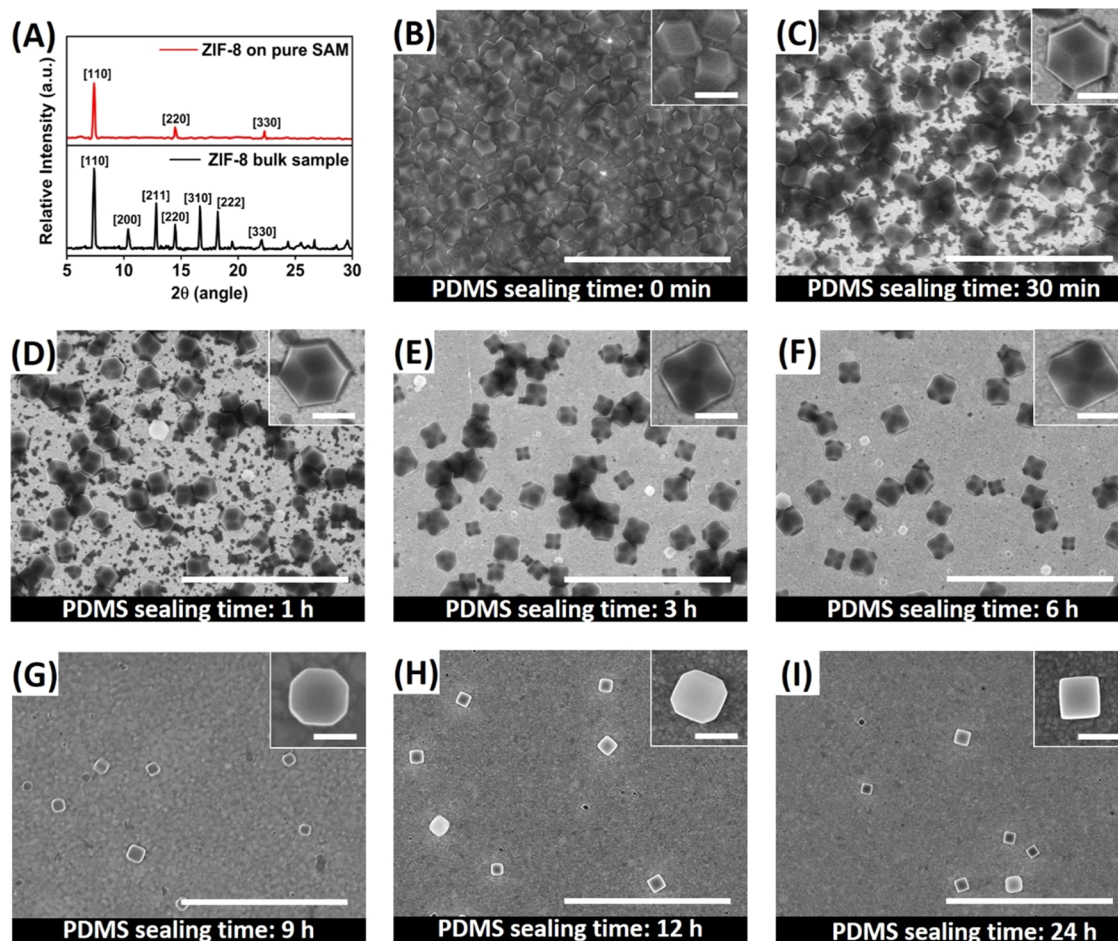
Figure 1. ZIF-8 crystal morphology evolution of different artificial molecular matrices immersed into a mixture of freshly prepared $Zn(NO_3)_2 \cdot 6H_2O$ (0.5 mL, 0.3 M) and 2-methylimidazole (10 mL, 1 M) aqueous solution at room temperature for 30 min. (A) XRD pattern (background corrected) of ZIF-8 bulk sample (black) and ZIF-8 grown on the pure MCU SAM-covered surface (red). (B−I) Morphological evolution of ZIF-8 grown on post-lift-off MCU SAM-covered surfaces under different PDMS contact sealing times: (B) 0 min, (C) 30 min, (D) 1 h, (E) 3 h, (F) 6 h, (G) 9 h, (H) 12 h, and (I) 24 h. Scale bars are 5 μm (0.5 μm in insets).

process. Importantly, the resulting specific MOF shapes can act as templates to support onsite ligand-free metal cluster growth. Unique fluorescence optical performance is observed depending on not only metal types but also MOF crystal geometry entailed facets.

RESULTS AND DISCUSSION

To generate diverse artificial molecular matrices for the unique additive-free MOF morphology growth control, an alkanethiol SAM-covered Au substrate is used as the solid support and the SAM density is modulated through a finely tunable selective molecule removal process. For demonstration, ZIF-8, which is used extensively as catalysts and functional biomaterials, is tested. As depicted in Scheme 1, a poly(dimethylsiloxane) (PDMS) stamp activated with 50 s of oxygen plasma treatment is conformally sealed onto a 11-mercaptoundecanol (MCU) SAM premodified Au substrate. Hydrophilic group-terminated MCU molecules strongly interact with the activated PDMS surface to initiate a contact-induced interface reaction. The interfacial covalent bond formation results in the partial removal of Au thiolates and creates artificial matrix defects when the stamp is separated from the Au surface.[49] This post lift-off Au substrate is thereafter immersed into a freshly prepared aqueous solution containing 2-methylimidazole and

zinc nitrate at room temperature for 30 min (see Supporting Information and Figure S1 for detailed experimental procedures). In this operation, the substrate is placed facing down to eliminate gravimetric sedimentation of colloidal MOF particles onto the SAM surface. Due to different matrix environments created from distinct molecule quantity removals, preferential MOF facet selections occur in the growth process and lead to the final differential MOF geometries on the Au surface. It should be noted that the formation of different MOF morphologies in this approach requires no addition of other additives in the process but only a suitable molecular environment.

Molecular Matrix-Guided MOF Crystal Morphology Controls

Based on this surface-guiding strategy, a variety of ZIF-8 MOF crystal morphologies are created on the Au surface depending on specific surface conditions (Figure 1). As shown in Figure 1A,B, a dense layer of homogeneous ZIF-8 crystals is formed on a hydroxyl-terminated SAM-covered Au surface. The characterization under X-ray diffraction (XRD) reveals an identical pattern of the obtained ZIF-8 MOFs (Figure 1A, top) compared to the ZIF-8 single crystal result (Figure 1A, bottom). Clear peak positions of the [110], [220], and [330] planes indicate the high phase purity and crystallinity of the
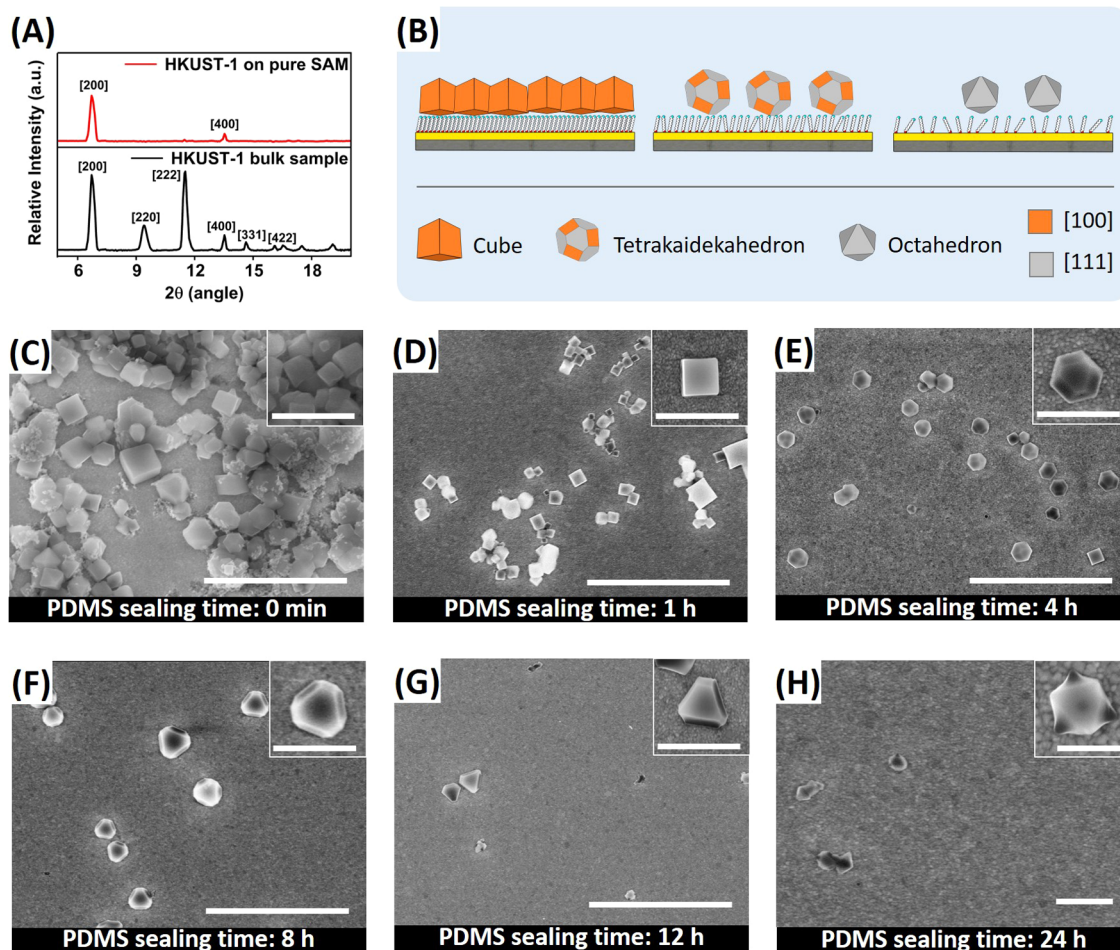
Figure 2. HKUST-1 crystal morphology evolution on different artificial molecular matrices. (A) XRD pattern (background corrected) of HKUST-1 bulk sample (black) and HKUST-1 grown on the pure MCU SAM-covered surface (red). (B) Schematic illustration of the monolayer artificial defect matrix resulted HKUST-1 MOF morphology changes via preferential facet selections between the [100, orange] and [111, gray] planes. (C−H) Morphological evolution of HKUST-1 grown on post-lift-off MCU SAM-covered surfaces under different PDMS contact sealing times: (C) 0 min, (D) 1 h, (E) 4 h, (F) 8 h, (G) 12 h, (H) 24 h. Scale bars are 5 μm in (C-G) and 1 μm in (H) (1 μm in insets of (C-G) and 0.2 μm in the inset of (H)).

obtained MOFs with a preferential crystal growth on the surface. Interestingly, intensities of other diffraction peaks are much weaker on these MOFs, pointing to a surface-decided crystal face selection over ZIF-8. In this case, the SAM surface-exposed hydroxyl tail groups can interact with precursor metal ions in the growth process and lead to an interfacial coordination between these two moieties.[50] These two-dimensionally (2D) assembled hydroxyl groups on the surface therefore support MOF crystalline formation along the plane, and a predominated crystal growth on the substrate is obtained.

Due to the aforementioned interface molecular interaction-dependent properties, this surface-guided crystal growth process can be altered if a local environment is modulated. To create adjustable molecular matrices, an oxygen plasma-activated PDMS stamp is utilized to initiate different levels of interfacial reactions toward the hydroxyl-terminated SAM through conformal contact time changes. When a longer contact time is employed, more interfacial reactions are completed and less alkanethiol molecules remain on the surface after PDMS stamp removal.[51] In other words, more randomly distributed defect sites are generated in the molecular matrix, and varieties of artificial matrices can

consequently be created.[47] Substrates prepared by this approach are utilized to support ZIF-8 growth by immersing them in a mixture of freshly prepared $Zn(NO_3)_2 \cdot 6H_2O$ (0.5 mL, 0.3 M) and 2-methylimidazole (10 mL, 1 M) aqueous solution at room temperature for 30 min, and the resulting MOF crystals are demonstrated in Figure 1C−I. Importantly, a pure type of ZIF-8 shape is found in each surface condition, and a morphology evolution process is observed along with stamp contact time changes. With the increase of PDMS stamp seal time, the morphology of surface-supported ZIF-8 gradually changes from rhombic dodecahedron, truncated rhombic dodecahedron, and truncated cube, to cube shapes. When only 30 min of contact seal is employed (Figure 1C), discrete and uniform rhombic dodecahedron crystals with an average size of 826 $\pm$ 10 nm (N = 150) are obtained. The crystals are also found dispersed over a monolayer configuration different from a thick layer formation with random crystal stacking (Figure 1B). With 1 h of sealing time (Figure 1D), larger rhombic dodecahedron crystals with exposed [110] facets and an average size of 830 $\pm$ 11 nm (N = 90) are formed. This MOF morphology evolution can be further altered if the stamp contact time is further elongated, where a 3−6 h of contact sealing produces truncated rhombic dodecahedron sized 850 $\pm$

7 nm (Figure 1E, N = 45) and 841 ± 9 nm (Figure 1F, N = 30), with the mixed [100] and [110] facets. Interestingly, a 9 and 12 h of stamp contact time lead to truncated cube crystals with an average size of 666 ± 11 nm (Figure 1G, N = 9) and 654 ± 5 nm (Figure 1H, N = 7), respectively. This indicates the dominance of the [100] facet over the [110] facet at these conditions and a replacement of truncated rhombic dodecahedron with truncated cube shapes. At the extreme condition of 24 h sealing time, cubic crystals with six [100] facets (617 ± 6 nm, N = 6) rule the whole post-lift-off region and no other shape of crystal is observed (Figure 1I). It is therefore summarized that an increase of sealing time preferentially advances the growth of ZIF-8 four-membered ring windows over the six-membered ones at the surface. Meanwhile, the MOF crystal density also reduces with a longer contact sealing time, pointing to less surface growth sites for specific shapes due to a larger quantity of alkanethiol removal (Figure 1B−I).

To verify if this molecular matrix guiding approach is a universal strategy, HKUST-1, which is constructed from copper ions and benzene-1,3,5-tricarboxylic acid (BTC) linkers, is also tested (Figure 2). Similarly, Au substrates modified with hydroxyl-terminated SAM under different levels of Au−thiolate removal are used as the supporting substrates. These diverse molecular matrices are immersed into the aqueous copper nitrate solution, followed by the addition of ethanolic BTC solution and $NaOH_{(aq)}$. The substrate is also operated with a facing-down orientation and the growth process is kept at room temperature for 30 min. Without the molecule removal, an MCU-covered SAM surface results in the formation of a highly crystalline HKUST-1 layer (Figure 2A−C). Under XRD investigation, obvious peaks are found corresponding to the [200] and [400] planes compared to other diffraction peaks. This indicates that the HKUST-1 growth on hydroxyl-terminated SAM is also surface-dependent and that the change of interface environment could lead to similar morphology alteration effects as ZIF-8 crystals (Figure 2B).[41] As demonstrated in Figure 2D−H, stamp contact time is used as a parameter in controlling the morphology of HKUST-1 crystals. Compared to cubic crystal aggregates obtained on a pristine MCU SAM surface (Figure 2C), discrete cubic crystals with an average size of 453 ± 15 nm (N = 72) start to show when 1 h of contact sealing is employed (Figure 2D). Obvious crystal morphology change occurs when 4 to 8 h of sealing time is applied (Figure 2E,F). The products exhibit tetrakaidekahedral structures consisting of six [100] and eight [111] facets with mean sizes of 632 ± 17 nm (N = 23) and 561 ± 7 nm (N = 9). After 12 h of contact sealing (Figure 2G), the [111] facet growth dominates over the [100] plane, and the formation of octahedral crystal begins, producing a particle size of 470 ± 15 nm (N = 6). Under the extreme 24 h sealing time condition (Figure 2H), symmetric octahedral crystals containing all [111] facets with the size of 201 ± 3 nm (N = 4) are formed. These interesting results confirm the presence of a morphology evolution process on the surface when a different type of MOF is used. Finely tunable molecular matrices are therefore believed to provide preferential selections over crystal facet growth and can deliver MOF morphology controls via interface molecular interactions.

Surface-Dependent MOF Crystal Growth Mechanism

Relying on the aforementioned interesting observations, the working principle of this unique interface molecular-guiding MOF growth through our artificial matrix creation is proposed in Figure 3. For an alkanethiol monolayer, its main influence toward a dynamic MOF crystal growth is the exposed tail
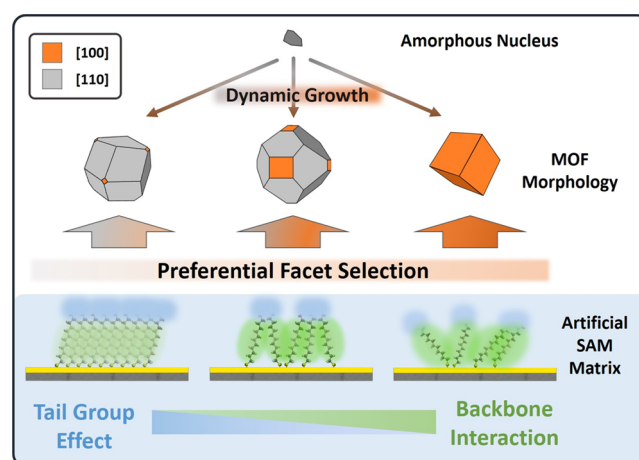

Figure 3. Schematic illustration of the integrated tail group regulation and backbone interaction induced preferential facet selection in the dynamic growth of ZIF-8.

groups. Interactions between these groups and the precursor components decide crystals' preferential growth planes along a surface. In the case of ZIF-8, surface hydroxyl groups provide the coordination capability to zinc ions and lead to the dominating [110] plane growth. Copious nucleus sites that ultimately result in rhombic dodecahedron crystals are therefore found on these surfaces. When an interface Au−thiolate removal operation is employed, the surface molecular matrix environment is tremendously changed. There are two main factors that need to be considered after a conditional Au−thiolate removal, i.e., the reduction of surface residue hydroxyl moieties and an increase of the alkane chain exposure. It has been proven that the interfacial chemical reaction between an oxygen plasma-activated PDMS stamp and the monolayer hydroxyl groups is contact-time-dependent.[49] The longer the duration is, the more molecules are removed from a Au surface after the lift-off process. X-ray photoelectron spectroscopy (XPS) spectra show that both the surface C and S contents are reduced when PDMS stamp sealing time is increased, indicating a reduced surface molecule coverage after lift-off (Figure S2). Randomly distributed residual alkanethiol quantities are therefore controllable and finely tunable molecular matrices with good alkane chain exposure can be produced.[46,51] In addition, partial removal of SAM should disrupt the original intermolecular interaction of adjacent thiol molecules, and a less-ordered molecular environment is therefore expected. In past MOF growth studies, capping agents, e.g., cetyltrimethylammonium bromide (CTAB), are required in preparation as the different facets' growth modulator for creating particular shapes. For example, the preferential adsorption of CTAB hydrocarbon chains onto hydrophobic ZIF-8 crystals in an aqueous solution slows down the crystal growth rate along the [100] direction and leads to cubic morphology.[52] From a similar perspective, a longer contact time exposes more hydrophobic alkane chains, which can function like CTAB molecules to hinder crystal growth rate along the [100] plane of MOF, resulting in smaller cubic ZIF-8 crystals. Moreover, the growth of HKUST-1 along the [111] direction is also accelerated by increasing CTAB concentrations in a precursor, and an octahedron shape is
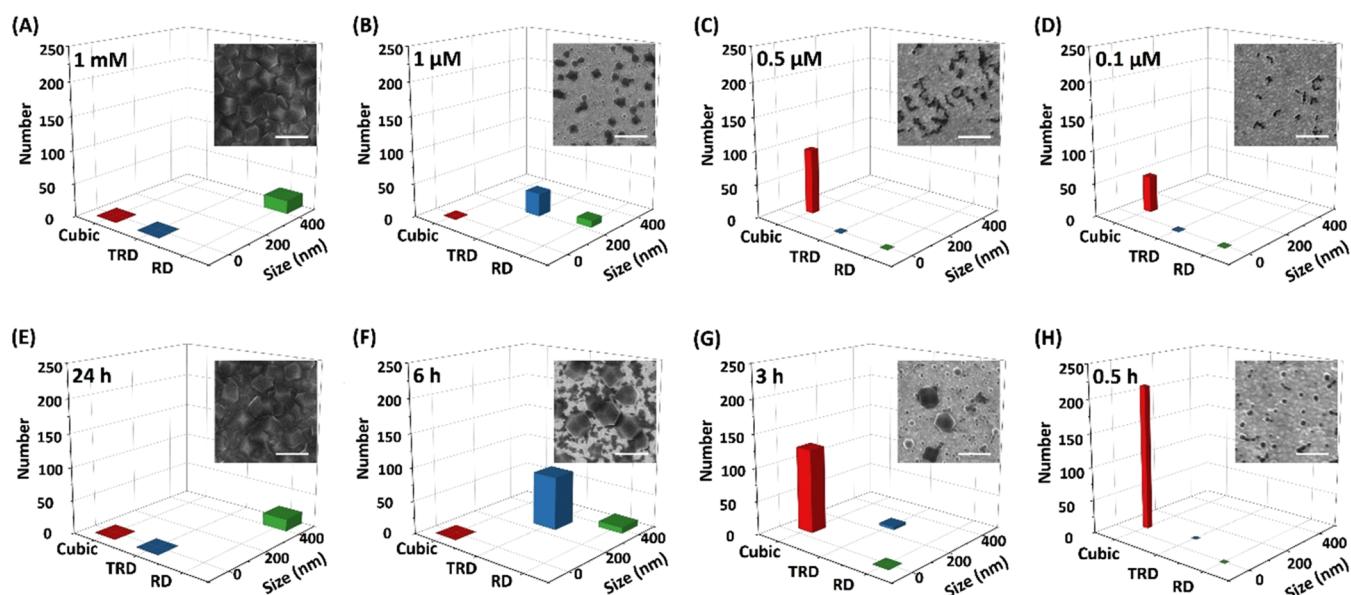
Figure 4. ZIF-8 crystals grown on natural defect-rich monolayers made with different thiol concentrations (A−D) or under different incubation times (E−H). SEM images of each condition and their corresponding graphical display (identical size of 5 μm × 5 μm area) of quantitative variables using 3D bar plot are shown: (A) 1 mM, (B) 1 μM, (C) 0.5 μM, (D) 0.1 μM, while the incubation time is fixed at 24 h; (E) 24 h, (F) 6 h, (G) 3 h, (H) 0.5 h, while the thiol concentration is fixed at 1 mM. Scale bar is 5 μm for (A, B, E, F); 3 μm for (C, G); and 2 μm for (D, H).

preferred as the final product.[22] Instead of introducing additional modulators to regulate MOF crystal growth, in this work, excellent selectivity over specific facets, i.e., [100] for ZIF-8 and [111] for HKUST-1, is achieved through adopting specific molecular matrices. Our surface-guiding approach supports the creation of diverse crystal morphologies without using any additional capping agents. The flexibility of our strategy is attributed to a mimicking environment provided by adjustable surface-exposed alkanethiol backbones through stamp conformal contact times. The balance between unremoved hydroxyl tails and exposed alkane chain backbones modulates an environment that preferentially adsorbs a particular crystal facet in the dynamic process. This slows down their crystal growth rates along a specific direction and leads to crystals with a particular morphology (Figure 3). To verify this, 6-mercapto-1-hexanol, a short-chain molecule, and 1-octadecanethiol, a long-chain molecule, are assembled on Au surfaces as supports for the nucleation of ZIF-8 crystals. In the case of 6-mercapto-1-hexanol SAM, no cubes are observed under any sealing conditions, implying that these short-chain molecules cannot grant control over MOF morphology due to the lack of backbone effect (Figure S3A,B). Besides, the formation of rhombic dodecahedron is also eliminated when the long-chain 1-octadecanethiol SAM is employed (Figure S3C,D), indicating the loss of tail group influence on MOF crystal growth control with these molecules. It is therefore concluded that competitive formations between the [110] and [100] planes of ZIF-8 result in shape changes from rhombic dodecahedron, truncated rhombic dodecahedron, and truncated cube to cube in this study (Figure 1). Similarly, the change of HKUST-1 crystal from cube and tetrakaidekahedron to octahedron, in Figure 2 originates from the competition of the [100] and [111] planes in the molecular matrix that influenced growth.

Since the crystal growth is a dynamic process, the formation environment temperature should play a key role in determining its final morphology,[53,54] a temperature-dependent investiga-

tion is therefore employed to investigate its effect on crystal formation. Under identical operation, a surface after 1 h of contact sealing but at 80 °C of growth condition (Figure S4A) produces a homogeneous ZIF-8 crystal film, similar to the result from the nontreated surface at room temperature (Figure 1B). Interestingly, uniform distributions of thermodynamically stable truncated rhombic dodecahedron crystals are obtained along with greatly reduced quantities when the PDMS sealing time is extended up to 12 h (Figure S4B−D). This decreasing trend of particle density is attributed to the reduced residual alkanethiol density on Au as nucleating sites. Nevertheless, the crystal morphology is maintained unlike results observed at room temperature (Figure 1D−H). It is expected that the environment temperature could potentially affect the growth kinetics of ZIF-8 crystals, and a higher temperature (higher total free energy) should lead to faster nucleation and crystallization rates with larger particle sizes.[55] On the other hand, the nuclei growth rate is strongly suppressed at a low temperature condition, and copious smaller particles are expected. As evidenced in Figure S4E−H, tiny, rough, and irregulate ZIF-8 agglomerates are observed when the system is operated at 4 °C. A similar quantity reduction trend along with PDMS sealing time is also observed, but no obvious crystalline structure is found on these surfaces. The representative results suggest different thermodynamics and kinetics-driven crystal growth routes governed by operation environments. When a higher temperature is applied, sufficient energy is provided to overcome the higher energy barrier due to the increased Gibbs free energy $\Delta G_v = -\frac{\Delta H_f(T_e - T)}{T_e}$, ΔG_v represents Gibbs free energy per unit volume [J/m^3], ΔH_f represents latent heat of fusion per unit volume [J/m^3], T_e represents solid−liquid equilibrium temperature [K], and T represents system temperature [K], and thermodynamically stable truncated rhombic dodecahedral crystals are formed.[56] Although an artificial molecular matrix is capable of guiding the specific facet growth, an increased

reaction rate at high temperatures diminishes the surface effect and the transformation of crystal morphology is prohibited. On the contrary, kinetically favored irregular agglomerates are always found at low temperatures due to Gibbs free energy reduction and a decreased reaction rate. An extremely slow growth process restrains crystalline formation, and similarly, the surface guiding contribution is also suppressed.

It is important to note that this unique molecular matrix-triggered approach brings a fundamental breakthrough in surface-guided MOF crystal morphology tuning with a straightforward and simple way, compared to conventional composition- or modulator-based strategies. Since this unique MOF crystal growth-guiding approach is interface molecular matrix dependent, several surface monolayer-controlling strategies are employed to investigate the underlying mechanism. Along with the Au−thiolate removal in our operation, residue alkanethiol molecules randomly distribute on the Au surface, and abundant artificial defects are left in the molecular matrix. The poor coverage of alkanethiol SAMs can be mimicked by two experimental conditions, i.e., the usage of lower alkanethiol concentration and a shortened surface incubation time. Constructing SAMs with a lower concentration of alkanethiol can lessen the kinetics of formation even with an overnight immersion, and monolayers with programmable defects can be obtained.[49] For instance, it has been demonstrated that SAMs formed in dilute alkanethiol solutions (∼1 μM) do not exhibit the same physical properties as those prepared in concentrated ones even after a week of immersion.[57] The alkanethiol precursor concentration is therefore first utilized to prepare SAM surfaces with a lower coverage for the MOF growth comparison. In these experiments, ZIF-8 MOFs are grown on Au substrates prepared using 1 mM, 1, 0.5, and 0.1 μM MCU solutions with an equal overnight immersion duration (Figure 4). Judging from SEM micrographs, dense rhombic dodecahedron ZIF-8 crystals are obtained with a fully covered SAM substrate (1 mM, Figure 4A), while comparatively smaller and discrete truncated rhombic dodecahedrons are observed when the thiol concentration is reduced to 1 μM (Figure 4B). Further lowering the thiol solution concentration (0.5 and 0.1 μM) produces a surface entailing heterogeneous nucleation of tiny and imperfectly edged ZIF-8 cubic crystallites (Figure 4C,D), presumably due to the very low coverage of thiol molecules. To summarize these results, a graphical display of quantitative variables using a 3D bar plot is employed. Two interesting phenomena are observed in these trials, including the shrinkage of particle size and the transformation of crystal morphology along with the thiol concentration reduction. Since the ZIF-8 [110] plane prefers to interact with the hydroxyl tail of an alkanethiol molecule, which is the nucleus site, a decrease of MOF formation quantity is consequently expected. Besides, less hydroxyl group preferred [110] planes should be produced and the existence of monolayer defects with increased alkane chain exposure could advance other preferential plane growth. This change of interface molecular environment explains the alteration of surface-dominating MOF morphologies from the [110] plane dominated rhombic dodecahedrons to the [100] plane governed cubes.

The other parameter used to manipulate the surface molecular environment is the SAM formation time. It has been demonstrated that an insufficient thiol solution incubation duration would lead to lower surface coverage and less-ordered molecular alignment accompanying copious

defects on Au.[58] This parameter is therefore also utilized to create imperfect monolayer matrices for MOF growth observation. A fixed 1 mM MCU concentration is applied in this test, while the substrate immersion time is varied from overnight to 30 min. Initially, a homogeneous layer of large rhombic dodecahedrons is observed when 24 h incubation time is applied (Figure 4E). When the immersion time is reduced to 6 h (Figure 4F), the majority of crystals tend to shrink in size, and truncated rhombic dodecahedrons dominate the surface. This shape of ZIF-8 tremendously diminishes, but copious cubes are formed when the incubation is shortened to 3 h (Figure 4G). Finally, with 0.5 h of substrate immersion time, uniform and discrete small cubic ZIF-8 crystals grow on the surface (Figure 4H). Similar to the effects observed in the thiol concentration variation experiments, the alteration of MOF crystal morphology and size in Figure 4E−H follows an identical trend. The hydroxyl tail-induced ZIF-8 [110] plane preferential growth reduces with shortened SAM formation time, and a lowered surface molecule coverage with defects leads to the [100] plane-dominated smaller cubes. Therefore, the inherent properties of the SAM used are also important for the morphology control of ZIF-8 crystals. When we compare results obtained from the thiol concentration and surface incubation time experiments with controllable molecular matrix achievements in Figure 1, three important observations can be concluded. First, the surface-supported MOF crystal growth changes have a similar tendency between naturally formed imperfect SAMs and artificially created matrices. Second, the substrate-guided MOF crystal morphology is surface monolayer coverage and distribution dependent. Third, the tunable matrices entailing artificial defects offer more precise and diverse controls over the MOF crystal growth morphology than naturally formed imperfect SAMs.

Ligand-Free Metal Nanocluster Synthesis on MOFs and Their Unique Optical Performance

The alteration of MOF crystal morphology may require the use of capping agents for selective crystalline growth controls. However, the introduction of these moieties often reduces the active surface area of MOFs and affects their physical and chemical performance.[59,60] Specific precursor pairing or environment selection can be deployed to avoid this but nucleation kinetics and crystalline defect control are required.[20,61] Relying on our straightforward and universal additive-free surface-guiding MOF crystal growth strategy, unique property manipulation carried by these ligand-free MOF crystals is expected. Since MOF crystal is a highly porous structure, these sub-10 nm pores could act as a template to support metal nanocluster onsite growth and alignment. Taking ZIF-8 crystals formed in this work as an example, the nitrogen-rich imidazole ring can help attract metal ions and stabilize metal atoms after the reduction process for particle growth. The onsite reduced metal particle dimension should be confined by the MOF pores, and their arrangements are affected by the employed MOF crystal morphology. Notably, additional capping agents are not required due to the well-separated pores, and product particle aggregation can be avoided. To realize this design, Au, Ag, and Cu are independently tested on the platform supported by cubic-shaped ZIF-8 MOFs. In these experiments, a ZIF-8 MOF-decorated surface is immersed into metal ion precursor solutions with an upside-down orientation to avoid gravimetric sedimentation, followed by the addition of sodium borohy-
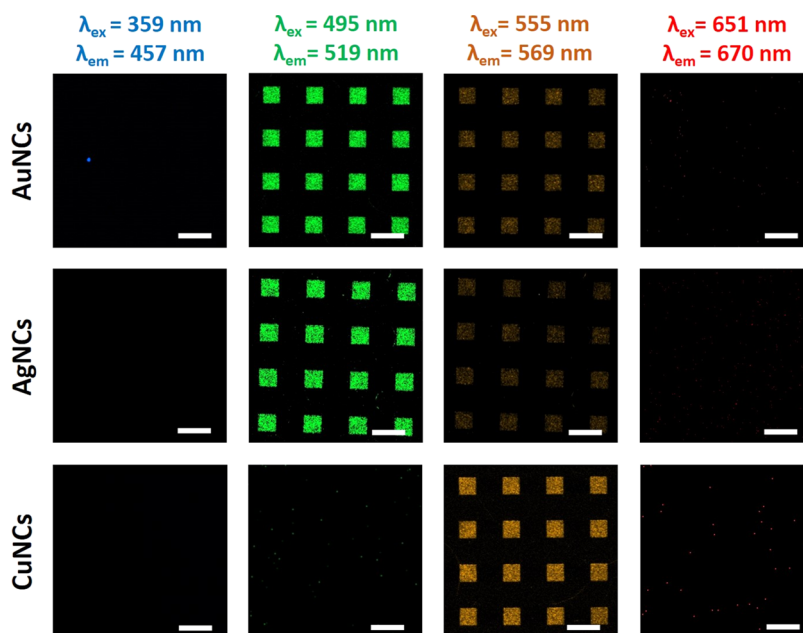
Figure 5. Fluorescence images of AuNCs, AgNCs, and CuNCs embedded cubic-shaped ZIF-8 MOF arrays. The scale bars are 100 μm.

dride. This operation initiates metal ion reductions within the porous structure, and metal clusters are formed embedding with the MOF crystal. The onsite reduction should happen quickly at crystal surface pores, and the formation of nanoclusters could block further diffusion of metal ions into the crystal interior. Meanwhile, the surplus of metal aggregates immediately precipitates out, and the solution color changes from light yellow to dark brown due to the lack of additional capping agents. Decoration of nanoclusters on exterior ZIF-8 surfaces is therefore anticipated while the dimension of clusters should be confined by the MOF crystal pore size. It should be noted that metal nanoclusters often exhibit unique optical properties and that the produced nanocluster-embedded MOFs should be no exception. To visualize this important characteristic, a prepatterned PDMS is used to create regions with different molecular matrices on the surface, where a 24 h of contact sealing (inside square areas) supports cubic-shaped ZIF-8 MOFs and uncontacted regions (outside square areas) entail a MOF layer similar to the 0 min sealing condition. Metal nanocluster formations are thereafter conducted on the patterned substrate, and the produced nanocluster-embedded MOFs are monitored under the epifluorescent microscope. As demonstrated in Figure 5, obvious fluorescence emissions corresponding to Au, Ag, and Cu reveal nanocluster formation on the MOF-patterned surface. Au nanoclusters (AuNCs)[62,63] and Ag nanoclusters (AgNCs)[64] give the most intense emission at 519 nm (under 495 nm excitation), while Cu nanoclusters (CuNCs)[65] deliver a strong emission at 569 nm (under 555 nm excitation). Other than the short-lived CuNC fluorescence, due to rapid oxidation without protection from capping agents (Video S1), fluorescence signals from AgNC and AuNC on this surface are stable for up to 2 weeks under ambient conditions. Weaker emissions at 569 nm (under 555 nm excitation) are also observed on AuNC and AgNC arrays, which are attributed to interparticle interactions between nanocluster-induced red shift.[66−68]

To exclude the possibility of the fluorescence being from sources other than metal nanoclusters embedded in MOFs, a series of control experiments are performed. First, different

MCU SAM molecular matrices are prepared, including nontreated, after 6, 12, and 24 h of stamp sealing conditions. Without the growth of MOF on these matrices, the identical AuNC growth process leads to nonfluorescent surfaces (Figure S5A), indicating no direct AuNC formation on a molecular matrix. Moreover, no fluorescence emission is observed if the MCU SAM after 24 h of stamp sealing is treated with Zn^{2+} ion or 2-methylimidazole, followed by the identical AuNC growth process (Figure S5B). This indicates that AuNC cannot form on surfaces with independent MOF precursor components. Finally, a surface-rich cubic MOFs but without the AuNC growth process delivers no fluorescence signal (Figure S5C), eliminating the fluorescent contribution to be from MOF crystals. Standing on these results, the observed fluorescence signals are attributed to metal nanoclusters embedded on the MOF crystals. Energy-dispersive X-ray (EDX) elemental mapping is also applied to characterize the metal nanocluster distribution on the surface, where AgNC is selected for demonstration to avoid the Au background interference on AuNC and oxidation impact on CuNC signals. Interestingly, Ag is mainly located inside the post-lift-off region, and its quantity reduces with MOF crystal amounts (the same trend as Zn signals) as PDMS sealing time elongates (Figure S6). This result points to a selective metal nanocluster formation on individual MOF crystals, presumably due to their highly exposed porous faces compared to a rough surface layer with more compact crystals. Nevertheless, the most exposed top face of a dense MOF layer at the original SAM-covered regions may still support the formation of metal clusters but with a relatively low quantity.

Taking advantage of this ligand-free metal nanocluster formation on MOF crystal and our surface-guided MOF morphology tunability, an interesting but previously unachievable task can be realized, i.e., MOF shape-dependent metal nanocluster aligning and their corresponding property investigation. Molecular matrices supporting the formation of rhombic dodecahedron (1 h of stamp sealing), truncated rhombic dodecahedron (3 h of stamp sealing), truncated cube (12 h of stamp sealing), and cube (24 h of stamp sealing)

shapes of ZIF-8 MOF are created, while AuNC and AgNC are independently grown on top of these geometries. Due to various faces entailed by distinct MOF geometries, the alignment of metal nanoclusters on each crystal shape should be different, and the resulting optical performance is expected to be unique. The aforementioned patterning approach is utilized to create AuNC/AgNC embedded MOF arrays, and their optical properties are monitored under an epifluorescent microscope. By analyzing the relative intensity of the observed fluorescent patterns, the relationship between MOF crystal shapes (depending on stamp sealing time) and their representing fluorescence intensity is compared (Figure 6). It
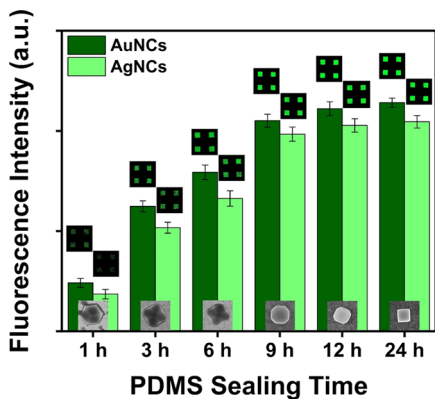

Figure 6. Shape-dependent fluorescence emission (at 519 nm, under 495 nm of excitation) behavior of AuNC- and AgNC-embedded ZIF-8 MOFs.

should be noted that the surface-supported MOF crystal quantity decreases as stamp sealing time increases (Figure 1), but surprisingly, MOFs embedded with AuNC or AgNC in this series of experiments deliver a reversed trend of fluorescence emission intensity. This phenomenon indicates an apparent dominating shape effect over the quantity influence, and is attributed to a nanocluster packing alignment induced fluorescence enhancement, which is cube > truncated cube > truncated rhombic dodecahedron > rhombic dodecahedron. To understand this effect, colloidal cubic and rhombic dodecahedral shape ZIF-8 MOFs are prepared and embedded with presynthesized AuNCs or AgNCs through coordination interactions (see the Supporting Information). The produced colloidal AuNCs@cubic ZIF-8 and AuNCs@rhombic dodecahedral ZIF-8 are compared with original AuNC and AgNC colloids (Figure S7), where an increase of fluorescence intensity is observed in both solutions. This effect is attributed to the aggregation-induced emission of nanoclusters, which reduces their collisions with solvents and restrains the vibration and rotation of excited nanoclusters.[66,69] Comparably, the cubic shape provides a stronger enhancement than the rhombic dodecahedron one in the colloidal system, which may help to conclude similar observations on a surface. Considering our surface-supported fluorescence enhancement, the distinct alignment of nanoclusters on MOFs tremendously changes their optical performance and can be independently evidenced along with the crystal face alteration. It is also observed that the size of the cubic crystals is smaller than rhombic dodecahedron ones, implying a shorter interparticle distance between nanoclusters, and a greater fluorescence enhancement is pronounced. This geometry-induced optical effect overwhelms other contributions even when their

quantity is one order of magnitude less, resulting in the unique shape-dependent fluorescence emission behavior in Figure 6. These exciting findings not only open a new door for precise morphology control over the synthesis of MOF crystals but they also extend numerous undiscovered phenomena to be further investigated.

■ CONCLUSIONS

In summary, an additive-free MOF crystal growth strategy with precisely controllable morphology changes is achieved by creating unique surface artificial molecular matrices. This approach provides a preferential MOF facet selection in its dynamic growth process, where distinct local intermolecular interactions decide the finally produced crystal shape. To generate a suitable molecular environment for this facet-guiding control, random surface molecule removal is accomplished by initiating chemical reactions between an activated PDMS stamp and an MCU SAM-covered Au surface with a subsequent stamp separation. This operation produces finely tunable molecular matrices rich in artificial defects, where the hydroxyl tail groups coordinate with precursor metal ions as nucleating sites and the distribution of exposed alkane chains helps to support the crystal growth along a specific direction. Modulation of complementary contributions from alkenthiol tails and backbones in a molecular matrix leads to preferential crystal facet selections on the dynamic route. Both ZIF-8 and HKUST-1 MOF generation are tested for technique demonstration, and the PDMS contact sealing time is used as the matrix creation ruler. A longer contact sealing time results in a larger quantity of removed molecules accompanying copious artificial defects in the matrix, and vice versa. These matrices support the ZIF-8 morphology changes from rhombic dodecahedron, truncated rhombic dodecahedron, and truncated cube to cube shapes as the [100] plane gradually dominates over the [110] plane along with the increasing PDMS sealing time. Similarly, the accelerated growth of HKUST-1 along the [111] direction over the [100] planes results in its shape changes, from cube, tetrakaidekahedron, to octahedron, when a longer contact sealing is applied. In addition to the nucleation guidance provided by an artificial molecular matrix, factors such as operation temperature can also influence the crystal morphology alteration. Relying on delicate controls over diverse MOF crystals' formation in this approach, the porous property of these structures is utilized in templating synthesis of ligand-free metal nanoclusters. Au, Ag, and Cu nanoclusters are formed embedding with ZIF-8 MOFs, while specific fluorescence emission properties are observed, depending on not only metal types but also employed MOF shapes. This MOF morphology-dependent metal nanocluster fluorescence emission follows the trend of cube > truncated cube > truncated rhombic dodecahedron > rhombic dodecahedron, which is attributed to a nanocluster packing alignment-induced fluorescence enhancement. Compared to quantity influences on a surface, the pronounced geometry factor dominates a metal nanocluster-embedded MOF's optical performance. These interesting findings reveal unachievable tasks and undiscovered phenomena based on our unique surface-guiding crystal growth and modulation. Meanwhile, this strategy provides an alternative thought on MOF morphology controls without the need for additives and opens a new door for other material syntheses with accompanying property changes and perspective applications.

■ METHODS

Materials

11-Mercaptoundecanol (MCU), 6-mercapto-1-hexanol, 1-octadecanethiol, hydrogen tetrachloroaurate(III) trihydrate ($HAuCl_4 \cdot 3H_2O$), silver nitrate ($AgNO_3$), 3-mercaptopropionic acid (MPA), and cetyltrimethylammonium bromide (CTAB) were purchased from Sigma-Aldrich (St. Louis, MO). Zinc nitrate hexahydrate ($Zn(NO_3)_2 \cdot 6H_2O$), copper nitrate trihydrate ($Cu(NO_3)_2 \cdot 3H_2O$), copper sulfate pentahydrate ($CuSO_4 \cdot 5H_2O$), sodium hydroxide (NaOH), sodium borohydride ($NaBH_4$), and sodium bicarbonate ($NaHCO_3$) were obtained from SHOWA Chemical Co., Ltd. (Tokyo, Japan). 2-Methylimidazole, benzene-1,3,5-tricarboxylic acid (BTC), and hexamethyldisilazane (HMDS) were purchased from Acros Organics (Geel, Belgium). Silicon wafers were purchased from Mustec Corp. (Hsinchu, Taiwan). The SYLGARD 184 silicone elastomer base and curing agent were purchased from Dow Corning Co. (Midland, MI). Deionized (DI) water (>18 $M\Omega \cdot cm$) was obtained from the ELGA PURELAB classic system (Taipei, Taiwan).

Instruments

The stamp surface activation was carried out by an oxygen plasma cleaner (Harrick Plasma PDC-32G, Ithaca, NY). Scanning electron microscopy (SEM) and energy-dispersive spectroscopy (EDX) were conducted with a cold-field emission scanning electron microscope (Hitachi S-4800, Tokyo, Japan). X-ray photoelectron spectroscopy (XPS) measurements were performed with a PHI Quantes spectrometer (ULVAC-PHI, Inc., Japan) using monochromatic Al Kα (1486.6 eV) light source, while the total resolution of 0.1 eV and beam size of 200 μm were maintained for the measurements. The spectra had been corrected to the main peak of the gold 4f spectrum that was set to 83.95 eV. Fluorescence images were obtained by a Zeiss epifluorescent microscope (Axio Imager. M2, Carl Zeiss Microscopy, Jena, Germany). X-ray powder diffraction (X' Pert PRO PANalytical, Malvern, PA) pattern analysis for each crystal structure was conducted with Cu Kα radiation (λ = 1.5418 Å). Fluorescence spectra were obtained by a Spectramax i3X MultiMode 96-well microplate reader (Molecular Devices, Hong Kong).

Growth of ZIF-8 and HKUST-1 MOF Crystals on SAM Matrices

Silicon substrates with 100 nm thick Au and 5 nm Cr adhesive layer were prepared by thermal evaporation. The Au substrates were immersed in 1.0 mM MCU ethanolic solution overnight to form a self-assembled monolayer (SAM). After the MCU SAM formation, the substrates were washed with ethanol to remove excess MCU molecules and then blow-dried with nitrogen gas. PDMS stamps were fabricated using standard photolithography-created masters. A 10:1 mass ratio of the SYLGARD 184 silicone elastomer base and curing agent were thoroughly mixed, degassed under vacuum, cast onto HMDS-coated master molds, and cured on an aluminum-top hot plate at 80 °C overnight. The PDMS stamps were separated from the master molds, sequentially rinsed by acetone and isopropanol, and then blow-dried by nitrogen gas. The prepared stamps were activated by 50 s exposure to oxygen plasma at a power of 18 W with 0.5 mbar oxygen flow. Thereafter, the stamps were conformally sealed onto the MCU SAM-modified substrates for different durations. After the contact-sealed stamp separation, the Au substrates were immersed into a mixture of freshly prepared aqueous solutions of $Zn(NO_3)_2 \cdot 6H_2O$ (0.5 mL, 0.3 M) and 2-methylimidazole (10 mL, 1 M) with the substrate facing down at room temperature for 30 min. In the case of HKUST ($[Cu_3(BTC)_2]_n$) frameworks, the Au substrates were immersed into an aqueous solution of $Cu(NO_3)_2 \cdot 3H_2O$ (6 mL, 0.6 M), followed by the addition of ethanolic BTC (6 mL, 0.017 M) and NaOH(aq) (0.5 mL, 1 M) solutions, sequentially, at room temperature for 1 h. After incubation, the substrates were gently rinsed with deionized water and blow-dried with nitrogen gas. The surfaces decorated with ZIF-8 and HKUST crystals, independently, were characterized with SEM operating at 10 keV.

Optimization of ZIF-8 Precursor Recipe

To optimize the precursor concentrations for ZIF-8 MOF growth on specially encoded MCU-covered Au surfaces, four different Zn to 2-methylimidazole molar ratio conditions (0.3:0.25, 0.3:0.50, 0.3:1.0, and 0.3:2.0) with a fixed $Zn(NO_3)_2 \cdot 6H_2O$ concentration at 0.3 M were examined on substrates prepared under 1 h of PDMS contact sealing. As seen in Figure S1, flower-like structures were found at a lower molar ratio of 0.3:0.25, whereas multilayered 2D flake-shaped crystals were obtained under the ratio of 0.3:0.50. Furthermore, with increasing 2-methylimidazole molar concentrations, the typical sodalite-like rhombic dodecahedron structure and tiny rougher spherical structures were observed under 0.3:1.0 and 0.3:2.0 conditions, respectively. Due to the absence of higher thermal stability and porosity, flower- and flake-shaped polymorphs were ruled out of consideration. In addition, tiny rougher structures were also avoided due to their lack of crystallinity. Consequently, the Zn/2-methylimidazole = 0.3:1.0 condition was chosen in the following experiments.

Ligand-Free Metal Nanocluster Synthesis on Diverse MOF Crystals

Metal nanoclusters were synthesized in a ligand-free fashion by immersing the prepatterned ZIF-8 MOF-decorated substrates into 10 μL of 1.0 M metal ion precursor solutions ($HAuCl_{4(aq)}$, $AgNO_{3(aq)}$, and $CuSO_{4(aq)}$ for AuNCs, AgNCs, and CuNCs, respectively), added with 6240 μL of DI water, followed by the rapid addition of $NaBH_{4(aq)}$ (3750 μL, 40 mM). These substrates were operated with a facing-down orientation to avoid direct particle deposition, while excess metal aggregates precipitated out and the solutions immediately changed color from light yellow to dark brown after the addition of $NaBH_4$. The produced nanocluster-embedded MOF decorating substrates were washed with DI water and then blow-dried with nitrogen gas. Fluorescence properties of nanoclusters were monitored with an epifluorescent microscope.

Synthesis of Colloidal Cubic and Rhombic Dodecahedral ZIF-8 MOF

The synthetic procedure was based on a previously reported protocol with slight modifications.[23] In a typical experiment, cubic ZIF-8 was prepared by mixing an aqueous solution of $Zn(NO_3)_2 \cdot 6H_2O$ (6 mL, 24 mM) and 2-methylimidazole (6 mL, 1.32 M), followed by the fast addition of CTAB (0.725 mL, 1 mM). The solution was stirred for 5 min and left undisturbed at room temperature for another 15 min. On the other hand, rhombic dodecahedral ZIF-8 was prepared using solely the same concentration of $Zn(NO_3)_2 \cdot 6H_2O$ and 2-methylimidazole mixture at room temperature for 15 min. After the formation of rhombic dodecahedral ZIF-8, CTAB (0.725 mL, 1 mM) was added into the solution to maintain the total volume and chemical composition.

Synthesis of Colloidal Metal Nanoclusters and Their Conjugation with ZIF-8 MOF

Initially, an aqueous solution of $HAuCl_4 \cdot 3H_2O$ (10 μL, 100 mM) was diluted by DI water (1.46 mL) in a clean glass vial (solution A). In a separate vial, $NaHCO_3$ (0.24 M) was dissolved in 2 mL of DI water containing 20 μL of MPA and sonicated for 10 s for complete dissolution (solution B). Next, solution A was mixed with 30 μL of solution B (this step produces colloidal metal nanoclusters), followed by the addition of freshly prepared 0.5 mL of cubic ZIF-8 colloidal solution and 0.5 mL of rhombic dodecahedral ZIF-8 colloidal solution separately at room temperature. The solutions turned from a transparent pale-yellow solution to a colloidal white suspension with the immediate formation of AuNCs@cubic ZIF-8 and AuNCs@rhombic dodecahedral ZIF-8. Similar experimental conditions were followed to synthesize AgNCs@cubic ZIF-8 and AgNCs@rhombic dodecahedral ZIF-8, except $AgNO_3$ was used as a metal ion precursor instead of $HAuCl_4 \cdot 3H_2O$. Finally, fluorescence properties of both nanoclusters prepared from three independent batches were examined to verify their batch-to-batch reproducibility.

ASSOCIATED CONTENT

Supporting Information

The Supporting Information is available free of charge at https://pubs.acs.org/doi/10.1021/jacsau.2c00692.

Optimization of ZIF-8 crystal growth condition (Figure S1); XPS of MCU-coated Au substrates under lift-off (Figure S2); effects of different thiol molecules (Figure S3); temperature effect on ZIF-8 crystal growth (Figure S4); control experiments of fluorescence images (Figure S5); EDX analysis of AgNC distribution (Figure S6); fluorescence properties of AuNCs and AgNCs in colloidal systems (Figure S7) (PDF)

Changes of CuNC fluorescence property in ambient (Video S1) (AVI)

AUTHOR INFORMATION

Corresponding Author

Wei-Ssu Liao − *Department of Chemistry, National Taiwan University, Taipei 10617, Taiwan;* ⬤ orcid.org/0000-0002-5619-4997; Email: wsliaochem@ntu.edu.tw

Authors

Pubali Kar − *Department of Chemistry, National Taiwan University, Taipei 10617, Taiwan*

Chang-Ming Wang − *Department of Chemistry, National Taiwan University, Taipei 10617, Taiwan*

Chia-Li Liao − *Department of Chemistry, National Taiwan University, Taipei 10617, Taiwan*

Ta-Sheng Chang − *Department of Chemistry, National Taiwan University, Taipei 10617, Taiwan*

Complete contact information is available at:
https://pubs.acs.org/10.1021/jacsau.2c00692

Notes

The authors declare no competing financial interest.

ACKNOWLEDGMENTS

REFERENCES

(1) Yaghi, O. M.; O'Keeffe, M.; Ockwig, N. W.; Chae, H. K.; Eddaoudi, M.; Kim, J. Reticular synthesis and the design of new materials. *Nature* **2003**, *423*, 705−714.

(2) Park, K. S.; Ni, Z.; Cote, A. P.; Choi, J. Y.; Huang, R.; Uribe-Romo, F. J.; Chae, H. K.; O'Keeffe, M.; Yaghi, O. M. Exceptional chemical and thermal stability of zeolitic imidazolate frameworks. *Proc. Natl. Acad. Sci. U.S.A.* **2006**, *103*, 10186−10191.

(3) Howarth, A. J.; Liu, Y.; Li, P.; Li, Z.; Wang, T. C.; Hupp, J. T.; Farha, O. K. Chemical, thermal and mechanical stabilities of metal−organic frameworks. *Nat. Rev. Mater.* **2016**, *1*, No. 15018.

(4) Chen, Z.; Mian, M. R.; Lee, S. J.; Chen, H.; Zhang, X.; Kirlikovali, K. O.; Shulda, S.; Melix, P.; Rosen, A. S.; Parilla, P. A.; Gennett, T.; Snurr, R. Q.; Islamoglu, T.; Yildirim, T.; Farha, O. K. Fine-Tuning a Robust Metal-Organic Framework toward Enhanced Clean Energy Gas Storage. *J. Am. Chem. Soc.* **2021**, *143*, 18838−18843.

(5) Kreno, L. E.; Leong, K.; Farha, O. K.; Allendorf, M.; Van Duyne, R. P.; Hupp, J. T. Metal-organic framework materials as chemical sensors. *Chem. Rev.* **2012**, *112*, 1105−1125.

(6) Sun, Y.; Zheng, L.; Yang, Y.; Qian, X.; Fu, T.; Li, X.; Yang, Z.; Yan, H.; Cui, C.; Tan, W. Metal−Organic Framework Nanocarriers for Drug Delivery in Biomedical Applications. *Nano-Micro Lett.* **2020**, *12*, No. 103.

(7) Qian, Q.; Asinger, P. A.; Lee, M. J.; Han, G.; Mizrahi Rodriguez, K.; Lin, S.; Benedetti, F. M.; Wu, A. X.; Chi, W. S.; Smith, Z. P. MOF-Based Membranes for Gas Separations. *Chem. Rev.* **2020**, *120*, 8161−8266.

(8) Li, S.; Huo, F. Metal-organic framework composites: from fundamentals to applications. *Nanoscale* **2015**, *7*, 7482−7501.

(9) Wang, H. F.; Chen, L.; Pang, H.; Kaskel, S.; Xu, Q. MOF-derived electrocatalysts for oxygen reduction, oxygen evolution and hydrogen evolution reactions. *Chem. Soc. Rev.* **2020**, *49*, 1414−1448.

(10) Lu, W.; Wei, Z.; Gu, Z. Y.; Liu, T. F.; Park, J.; Park, J.; Tian, J.; Zhang, M.; Zhang, Q.; T, G.; M, B.; Zhou, H. C. Tuning the structure and function of metal−organic frameworks via linker design. *Chem. Soc. Rev.* **2014**, *43*, 5561−5593.

(11) Chui, S. S. Y.; Lo, S. M. F.; Charmant, J. P. H.; Orpen, A. G.; Williams, L. D. A Chemically Functionalizable Nanoporous Material $[Cu_3(TMA)_2(H_2O)_3]_n$. *Science* **1999**, *283*, 1148−1150.

(12) Wang, C. M.; Kim, J.; Tang, J.; Kim, M.; Lim, H.; Malgras, V.; You, J.; Xu, Q.; Li, J.; Yamauchi, Y. New Strategies for Novel MOF-Derived Carbon Materials Based on Nanoarchitectures. *Chem* **2020**, *6*, 19−40.

(13) Hwang, J.; Ejsmont, A.; Freund, R.; Gosci anska, J.; Schmidt, B.; Wuttke, S. Controlling the morphology of metal-organic frameworks and porous carbon materials: metal oxides as primary architecture-directing agents. *Chem. Soc. Rev.* **2020**, *49*, 3348−3422.

(14) Ko, M.; Mendecki, L.; Mirica, K. A. Conductive two-dimensional metal-organic frameworks as multifunctional materials. *Chem. Commun.* **2018**, *54*, 7873−7891.

(15) Kalaj, M.; Cohen, S. M. Postsynthetic Modification: An Enabling Technology for the Advancement of Metal-Organic Frameworks. *ACS Cent. Sci.* **2020**, *6*, 1046−1057.

(16) Wang, Z.; Cohen, S. M. Postsynthetic Covalent Modification of a Neutral Metal-Organic Framework. *J. Am. Chem. Soc.* **2007**, *129*, 12368−12369.

(17) Wang, C.; Cheng, P.; Yao, Y.; Yamauchi, Y.; Yan, X.; Li, J.; Na, J. In-situ fabrication of nanoarchitectured MOF filter for water purification. *J. Hazard. Mater.* **2020**, *392*, No. 122164.

(18) Schejn, A.; Balan, L.; Falk, V.; Aranda, L.; Medjahdi, G.; Schneider, R. Controlling ZIF-8 nano- and microcrystal formation and reactivity through zinc salt variations. *CrystEngComm* **2014**, *16*, 4493−4500.

(19) Troyano, J.; Carne-Sanchez, A.; Avci, C.; Imaz, I.; Maspoch, D. Colloidal metal-organic framework particles: the pioneering case of ZIF-8. *Chem. Soc. Rev.* **2019**, *48*, 5534−5546.

(20) Jian, M.; Liu, B.; Liu, R.; Qu, J.; Wang, H.; Zhang, X. Water-based synthesis of zeolitic imidazolate framework-8 with high morphology level at room temperature. *RSC Adv.* **2015**, *5*, 48433−48441.

(21) Yang, F.; Mu, H.; Wang, C. M.; Xiang, L.; Yao, K. X.; Liu, L.; Yang, Y.; Han, Y.; Li, Y.; Pan, Y. Morphological Map of ZIF-8 Crystals with Five Distinctive Shapes: Feature of Filler in Mixed-Matrix Membranes on C_3H_6/C_3H_8 Separation. *Chem. Mater.* **2018**, *30*, 3467−3473.

(22) Liu, Q.; Jin, L. N.; Sun, W. Y. Facile fabrication and adsorption property of a nano/microporous coordination polymer with controllable size and morphology. *Chem. Commun.* **2012**, *48*, 8814−8816.

(23) Zheng, G.; Chen, Z.; Sentosun, K.; Perez-Juste, I.; Bals, S.; Liz-Marzan, L. M.; Pastoriza-Santos, I.; Perez-Juste, J.; Hong, M. Shape control in ZIF-8 nanocrystals and metal nanoparticles@ZIF-8 heterostructures. *Nanoscale* **2017**, *9*, 16645−16651.

(24) Umemura, A.; Diring, S.; Furukawa, S.; Uehara, H.; Tsuruoka, T.; Kitagawa, S. Morphology design of porous coordination polymer

crystals by coordination modulation. *J. Am. Chem. Soc.* **2011**, *133*, 15506−15513.

(25) Wang, Z.; Ge, L.; Li, M.; Lin, R.; Wang, H.; Zhu, Z. Orientated growth of copper-based MOF for acetylene storage. *Chem. Eng. J.* **2019**, *357*, 320−327.

(26) Forgan, R. S. Modulated self-assembly of metal-organic frameworks. *Chem. Sci.* **2020**, *11*, 4546−4562.

(27) Benito, J.; Sorribas, S.; Lucas, I.; Coronas, J.; Gascon, I. Langmuir-Blodgett Films of the Metal-Organic Framework MIL-101(Cr): Preparation, Characterization, and CO_2 Adsorption Study Using a QCM-Based Setup. *ACS Appl. Mater. Interfaces* **2016**, *8*, 16486−16492.

(28) Shekhah, O.; Eddaoudi, M. The liquid phase epitaxy method for the construction of oriented ZIF-8 thin films with controlled growth on functionalized surfaces. *Chem. Commun.* **2013**, *49*, 10079−10081.

(29) Zhang, C.; Yan, J.; Ji, T.; Du, D.; Sun, Y.; Liu, L.; Zhang, X.; Liu, Y. Fabrication of highly (110)-Oriented ZIF-8 membrane at low temperature using nanosheet seed layer. *J. Membr. Sci.* **2022**, *641*, No. 119915.

(30) Zhang, S.; Wang, Z.; Ren, H.; Zhang, F.; Jin, J. Nanoporous film-mediated growth of ultrathin and continuous metal−organic framework membranes for high-performance hydrogen separation. *J. Mater. Chem. A* **2017**, *5*, 1962−1966.

(31) Kida, K.; Fujita, K.; Shimada, T.; Tanaka, S.; Miyake, Y. Layer-by-layer aqueous rapid synthesis of ZIF-8 films on a reactive surface. *Dalton Trans.* **2013**, *42*, 11128−11135.

(32) Bai, X. J.; Lu, X. Y.; Ju, R.; Chen, H.; Shao, L.; Zhai, X.; Li, Y. N.; Fan, F. Q.; Fu, Y.; Qi, W. Preparation of MOF Film/Aerogel Composite Catalysts via Substrate-Seeding Secondary-Growth for the Oxygen Evolution Reaction and CO_2 Cycloaddition. *Angew. Chem., Int. Ed.* **2021**, *60*, 701−705.

(33) Chen, H.; Zhang, W.; Li, M.; He, G.; Guo, X. Interface Engineering in Organic Field-Effect Transistors: Principles, Applications, and Perspectives. *Chem. Rev.* **2020**, *120*, 2879−2949.

(34) Lecot, S.; Lavigne, A.; Yang, Z.; Chevolot, Y.; Goutorbe, M. P.; Yeromonahos, C. Effects of the Chemical and Structural Properties of Silane Monolayers on the Organization of Water Molecules and Ions at Interfaces, from Molecular Dynamics Simulations. *Langmuir* **2021**, *37*, 5563−5572.

(35) Kim, W.; Park, J. H.; Hwang, H. J.; Rim, Y. S.; Choi, D. Interfacial molecular engineering for enhanced polarization of negative tribo-materials. *Nano Energy* **2022**, *96*, No. 107110.

(36) Choi, I.; Yeo, W. S. Self-assembled monolayers with dynamicity stemming from (bio)chemical conversions: from construction to application. *ChemPhysChem* **2013**, *14*, 55−69.

(37) Hermes, S.; Schroder, F.; Chelmowski, R.; Woll, C.; Fischer, R. A. Selective Nucleation and Growth of Metal-Organic Open Framework Thin Films on Patterned COOH/CF3-Terminated Self-Assembled Monolayers on Au(111). *J. Am. Chem. Soc.* **2005**, *127*, 13744−13745.

(38) Singh, M.; Kaur, N.; Comini, E. Role of Self-Assembled Monolayers in Electronic Devices. *J. Mater. Chem. C* **2020**, *8*, 3938−3955.

(39) Li, S.; Wang, Y.; Zhang, Z.; Wang, Y.; Li, H.; Xia, F. Exploring End-Group Effect of Alkanethiol Self-Assembled Monolayers on Electrochemical Aptamer-Based Sensors in Biological Fluids. *Anal. Chem.* **2021**, *93*, 5849−5855.

(40) Lu, G.; Farha, O. K.; Zhang, W.; Huo, F.; Hupp, J. T. Engineering ZIF-8 thin films for hybrid MOF-based devices. *Adv. Mater.* **2012**, *24*, 3970−3974.

(41) Biemmi, E.; Scherb, C.; Bein, T. Oriented Growth of the Metal Organic Framework $Cu_3(BTC)_2(H_2O)_3 \cdot xH_2O$ Tunable with Functionalized Self-Assembled Monolayers. *J. Am. Chem. Soc.* **2007**, *129*, 8054−8055.

(42) Conato, M. T.; Jacobson, A. J. Control of nucleation and crystal growth kinetics of MOF-5 on functionalized gold surfaces. *Microporous Mesoporous Mater.* **2013**, *175*, 107−115.

(43) Cubillas, P.; Anderson, M. W.; Attfield, M. P. Crystal Growth Mechanisms and Morphological Control of the Prototypical Metal−Organic Framework MOF-5 Revealed by Atomic Force Microscopy. *Chem. - Eur. J.* **2012**, *18*, 15406−15415.

(44) Chen, C. Y.; Li, H. H.; Chu, H. Y.; Wang, C. M.; Chang, C. W.; Lin, L. E.; Hsu, C. C.; Liao, W. S. Finely Tunable Surface Wettability by Two-Dimensional Molecular Manipulation. *ACS Appl. Mater. Interfaces* **2018**, *10*, 41814−41823.

(45) Shuster, M. J.; Vaish, A.; Szapacs, M. E.; Anderson, M. E.; Weiss, P. S.; Andrews, A. M. Biospecific Recognition of Tethered Small Molecules Diluted in Self-Assembled Monolayers. *Adv. Mater.* **2008**, *20*, 164−167.

(46) Liao, W. S.; Cheunkar, S.; Cao, H. H.; Bednar, H. R.; Weiss, P. S.; M, A. A. Subtractive Patterning via Chemical Lift-Off Lithography. *Science* **2012**, *337*, 1517−1521.

(47) Chen, C. Y.; Wang, C. M.; Chen, P. S.; Liao, W. S. Self-standing aptamers by an artificial defect-rich matrix. *Nanoscale* **2018**, *10*, 3191−3197.

(48) Cao, H. H.; Nakatsuka, N.; Serino, A. C.; Liao, W. E.; Cheunkar, S.; Yang, H.; Weiss, P. S.; Andrews, A. M. Controlled DNA Patterning by Chemical Lift-Off Lithography: Matrix Matters. *ACS Nano* **2015**, *9*, 11439−11454.

(49) Chen, C. Y.; Wang, C. M.; Chen, P. S.; Liao, W. S. Surface functional DNA density control by programmable molecular defects. *Chem. Commun.* **2018**, *54*, 4100−4103.

(50) Shekhah, O.; Liu, J.; Fischer, R. A.; Woll, C. MOF thin films: existing and future applications. *Chem. Soc. Rev.* **2011**, *40*, 1081−1106.

(51) Chen, C.-Y.; Chang, C.-H.; Wang, C.-M.; Li, Y.-J.; Chu, H.-Y.; Chan, H.-H.; Huang, Y.-W.; Liao, W.-S. Large Area Nanoparticle Alignment by Chemical Lift-Off Lithography. *Nanomaterials* **2018**, *8*, No. 71.

(52) Pan, Y.; Heryadi, D.; Zhou, F.; Zhao, L.; Lestari, G.; Su, H.; Lai, Z. Tuning the crystal morphology and size of zeolitic imidazolate framework-8 in aqueous solution by surfactants. *CrystEngComm* **2011**, *13*, 6937−6940.

(53) Wu, Z.; Yang, S.; Wu, W. Application of temperature cycling for crystal quality control during crystallization. *CrystEngComm* **2016**, *18*, 2222−2238.

(54) Aulakh, D.; Varghese, J. R.; Wriedt, M. The Importance of Polymorphism in Metal-Organic Framework Studies. *Inorg. Chem.* **2015**, *54*, 8679−8684.

(55) Desiraju, G. R.; Vittal, J. J.; Ramanan, A. *Crystal Engineering*; World Scientific, 2011; p 232.

(56) Mulin, J. W. *Crystallization*, 4th ed.; Butterworth−Heinemann: Oxford, 2001.

(57) Bain, C. D.; Troughton, E. B.; Tao, Y. T.; Evall, J.; Whitesides, G. M.; Nuzzo, R. G. Formation of monolayer films by the spontaneous assembly of organic thiols from solution onto gold. *J. Am. Chem. Soc.* **1989**, *111*, 321−335.

(58) Stranick, S. J.; Parikh, A. N.; Tao, Y. T.; Allara, D. L.; Weiss, P. S. Phase Separation of Mixed-Composition Self-Assembled Monolayers into Nanometer Scale Molecular Domains. *J. Phys. Chem* **1994**, *98*, 7636−7646.

(59) Liu, H.; Chang, L.; Chen, L.; Li, Y. In situ one-step synthesis of metal−organic framework encapsulated naked Pt nanoparticles without additional reductants. *J. Mater. Chem. A* **2015**, *3*, 8028−8033.

(60) Jiang, D.; Mallat, T.; Krumeich, F.; Baiker, A. Polymer-assisted synthesis of nanocrystalline copper-based metal−organic framework for amine oxidation. *Catal. Commun.* **2011**, *12*, 602−605.

(61) Stavila, V.; Volponi, J.; Katzenmeyer, A. M.; Dixon, M. C.; Allendorf, M. D. Kinetics and mechanism of metal−organic framework thin film growth: systematic investigation of HKUST-1 deposition on QCM electrodes. *Chem. Sci.* **2012**, *3*, 1531−1540.

(62) Kawasaki, H.; Hamaguchi, K.; Osaka, I.; Arakawa, R. ph-Dependent Synthesis of Pepsin-Mediated Gold Nanoclusters with Blue Green and Red Fluorescent Emission. *Adv. Funct. Mater* **2011**, *21*, 3508−3515.

(63) Kar, P.; Chang, T. S.; Chen, C. Y.; Chen, J. S.; Yi, S.; Sutradhar, S.; Liao, W. S. Fluorescence Turn-On Antioxidant Recognition by Interface-Mediated Radical Termination of L-Cysteine-Capped Gold Nanoclusters. *ACS Appl. Nano Mater.* **2021**, *4*, 3360−3368.

(64) Yourston, L.; Rolband, L.; West, C.; Lushnikov, A.; Afonin, K. A.; Krasnoslobodtsev, A. V. Tuning properties of silver nanoclusters with RNA nanoring assemblies. *Nanoscale* **2020**, *12*, 16189−16200.

(65) Deng, H. H.; Zhuang, Q. Q.; Huang, K. Y.; Balasubramanian, P.; Lin, Z.; Peng, H. P.; Xia, X. H.; Chen, W. Solid-state thiolate-stabilized copper nanoclusters with ultrahigh photoluminescence quantum yield for white light-emitting devices. *Nanoscale* **2020**, *12*, 15791−15799.

(66) Luo, Z.; Yuan, X.; Yu, Y.; Zhang, Q.; Leong, D. T.; Lee, J. Y.; Xie, J. From Aggregation-Induced Emission of Au(I)−Thiolate Complexes to Ultrabright Au(0)@Au(I)−Thiolate Core−Shell Nanoclusters. *J. Am. Chem. Soc.* **2012**, *134*, 16662−16670.

(67) Huang, H. Y.; Ca, K. B.; Io, C. C.; Chen, P. W.; Soebroto, R. J.; Shen, J. L.; Yeh, J. M.; Yuan, C. T. Electronically Coupled Gold Nanoclusters Render Deep-Red Emission with High Quantum Yields. *J. Phys. Chem. Lett.* **2020**, *11*, 9344−9350.

(68) Sun, P.; Wang, Z.; Bi, Y.; Sun, D.; Zhao, T.; Zhao, F.; Wang, W.; Xin, X. Self-Assembly-Driven Aggregation-Induced Emission of Silver Nanoclusters for Light Conversion and Temperature Sensing. *ACS Appl. Nano Mater.* **2020**, *3*, 2038−2046.

(69) Xia, M.; Sui, Y.; Guo, Y.; Zhang, Y. Aggregation-induced emission enhancement of gold nanoclusters in metal-organic frameworks for highly sensitive fluorescent detection of bilirubin. *Analyst* **2021**, *146*, 904−910.